PAPER • OPEN ACCESS

Direct observation of dendrite fragmentation in the solidification of undercooled melts

View the article online for updates and enhancements.

IOP | ebooks™

Bringing you innovative digital publishing with leading voices to create your essential collection of books in STEM research.

Start exploring the collection - download the first chapter of every title for free.

Direct observation of dendrite fragmentation in the solidification of undercooled melts

Andrew M Mullis[1] & Nafisul Haque[1]

[1]School of Chemical and Process Engineering, University of Leeds, Leeds, UK

E-Mail: A.M.Mullis@leeds.ac.uk

Abstract. The fragmentation of dendrites immediately following the recalescence phase of growth during the solidification of undercooled melts has been invoked to explain various rapid solidification microstructures. Despite this, little direct evidence of such a fragmentation process usually survives in the as-solidified material. We report on the rapid solidification of the single phase, congruently melting intermetallic β-Ni$_3$Ge. During equilibrium solidification this material solidifies to the chemically ordered L1$_2$ crystal structure. Conversely, during rapid solidification, disorder trapping results in solidification to a random fcc solid solution, thereby providing a means to distinguish the rapidly solidified structures. We present results which show a range of microstructures in which the dendrite fragmentation process has been captured in progress. Results from EBSD Euler mapping reveal that dendrite fragmentation is a potential, but not particularly efficient, route to grain refinement.

1. Introduction

Spontaneous grain refinement (SGR) during the solidification of deeply undercooled melts has been a subject of enduring interest within rapid solidification. Defined as an abrupt reduction in grain size, typically of at least an order of magnitude, above a critical undercooling, ΔT^*, the first such observation was made by Walker in pure Ni in 1959 [1]. Since then many other pure metals [2, 3, 4] and alloys [5, 6, 7] have been observed to undergo similar transitions, with alloy systems often displaying a more complex behavior involving two distinct grain refinement transitions. For a typical alloy system undergoing SGR, a fine grained structure is observed above a lower SGR transition undercooling ΔT_1^*, reverting to a coarse grain structure at higher undercooling. In most systems a second episode of grain refinement is then observed at yet high undercooling, ΔT_2^*.

Where growth velocity measurements have been made, the onset of SGR above ΔT^* (ΔT_2^* in alloys) is often accompanied by a discontinuous break in the velocity-undercooling curve [2]. Below ΔT^*, the growth velocity, V, can generally be described by a power-law relationship of the form $V \propto (\Delta T^*)^\beta$, with β typically being in the range 2-3, while above ΔT^*, V is often linear in ΔT. High speed imaging of the solidification front has also suggested that there is a change in the front morphology from an angular euhederal morphology below ΔT^* to a smooth morphology above ΔT^* [8]. However, in alloy systems there is generally no signature in the velocity undercooling curve corresponding to the lower SGR transition at ΔT_1^*. This has prompted suggestions that the upper and lower SGR transitions have different origins [9, 10], an idea that ties in with some of the earliest observation of SGR in which it was noted that there were subtle difference in the solute segregation patterns observed at high and low undercoolings [11]. At high undercooling the solute segregation pattern is typically spheroidal, whereas

at low undercooling small, well-developed dendritic fragments are observed.

Numerous mechanisms have been proposed to account for SGR. Early theories included; copious nucleation ahead of the solidification front resulting from a shrinkage induced pressure pulse [1], the action of minor solute additions [12], and recrystallization [13]. However, perhaps the most enduring model for SGR is that of remelting and fragmentation of dendrites shortly after the recalescence phase of solidification, during which time the solid and liquid co-exist. Early proponents of fragmentation based models included Horvay [14] and Kattamis & Flemings [11], although perhaps the best known of these fragmentation models is that due to Schwarz *et al*. [15]. They argue, based upon a mathematical analysis due to Karma [16] for the growth of Rayleigh instabilities along the dendrite, that there are two key timescales to consider. The first is that for the breakup, τ_{br}. This is the timescale over which fragmentation and subsequent spheroidisation of secondary dendrite arms will occur during co-existence of the solid and liquid following recalescence. The second is the plateau timescale, τ_{pl}, which is the time for which the solid and liquid co-exist. If $\tau_{br} < \tau_{pl}$ then breakup is assumed to occur with the fragments providing nuclei for the subsequent growth of refined grains. τ_{pl} is simply a function of the heat extraction rate from the sample while τ_{br} is a function primarily of the size of the dendrite, which in turn, due to the self-similarity of dendrites, is equivalent to it being a function of the dendrite tip radius, ρ, with smaller radii giving shorter breakup times. Consequently, for a given cooling rate there is a critical tip radius, ρ^*, below which fragmentation occurs.

An attractive feature of the Schwarz model [15] is that it appears to give a natural explanation for there being only one SGR transition in pure metals and two in alloys; the tip radius decreasing monotonically in a pure metal but passing through a local minimum at intermediate undercoolings in alloy systems. There are however problems with the Schwarz model. It is for instance difficult to see how remelting, which by definition must occur post-recalescence, can give rise to either a break in the velocity-undercooling curve or a change in the morphology of the solidification front. That both occur concurrently with the onset of SGR must therefore be ascribed to coincidence. We have previously argued [17] that a change in the primary solidification morphology from dendritic to seaweed is therefore a more likely precursor to the onset of SGR, as this may also be expected to have a signature in both the morphology of the solidification front and the velocity-undercooling behavior. However, there is also a further objection to the Schwarz model for SGR. There is an implicit assumption that remelting and fragmentation of the dendrites formed during recalescence will lead to grain refinement. In fact, it is not at all clear that even if dendrite fragmentation and spheroidisation occurs as described by the model of Karma [16] that such fragments will subsequently nucleate the copious number of new grains required for SGR.

Unfortunately, direct experimental evidence of dendrite fragmentation in rapidly solidified metals has been extremely difficult to obtain as any indication of such fragmentation is usually obscured in the final, as-solidified sample. Such remelting has been predicted by [18] for 250 μm droplets of Al-10 wt% Cu alloy, wherein it was found that the fraction of the recalescence solid subject to remelting was a strong function of the nucleation undercooling, with high undercooling leading to greater remelting. Subsequent EBSD analysis of Al-Fe alloys [19] showed evidence of such remelting, with detached and slightly misoriented primary and secondary dendrite arms being observed.

Recently we have identified that remelting and fragmentation of the primary dendrites formed during recalescence may be preserved during rapid cooling of the congruently melting intermetallic compound β-Ni₃Ge. As such, β-Ni₃Ge is an interesting vehicle to probe whether remelting is a likely origin of SGR. Here we report on drop-tube experiments upon the β-Ni₃Ge compound.

2. Experimental Methods
β-Ni₃Ge is a congruently melting intermetallic with the $L1_2$ ordered fcc crystal structure and a homogeneity range of 22.5 to 25.0 at. % Ge [20]. The congruent melting temperature is 1405 K and upon slow cooling the compound will grow in the ordered form directly from the liquid. However, disorder trapping occurs for undercoolings in excess of 168 K [21].

The starting alloy for the drop-tube experiments was produced by arc-melting together Ni and Ge (both 99.99% purity) in the correct proportions under a protective Ar atmosphere with the resulting ingot being checked to ensure it was single phase β-Ni$_3$Ge using XRD (see below). For rapid solidification processing a 9.6 g ingot was melted by induction heating at the top of the Leeds 6.5 m drop-tube, which is maintained at a pressure of 50 kPa throughout processing. The sample is contained within an alumina crucible with three 300 μm laser drilled holes in the base. Ejection of the sample is occasioned by pressurizing the crucible to 400 kPa, wherein a fine spray of droplets is produced which solidify in flight down the tube. The melt ejection occurred at a temperature of 1480 K, corresponding to a melt superheat of 75 K. More details of the drop-tube method are given in [22].

Following drop-tube processing the powders are sieved into 9 standard size fraction between 850 μm and 38 μm. Each size fraction is subject to XRD analysis using a PANalytical Xpert Pro before being mounted in thermosetting resin, ground and polished to a 0.25 μm finish for microstructural analysis. In order to reveal the underlying microstructure samples were etched for 20 s using a highly aggressive mixture comprising equal parts of undiluted HF, HCl and HNO$_3$. Microstructural analysis was undertaken using a Carl Zeiss EVO MA15 Scanning Electron Microscope (SEM) equipped with an Oxford Instrument X-Max Energy-Dispersive X-Ray (EDX) detector. Electron Backscatter Diffraction (EBSD) was undertaken using a FEI Quanta 650 FEGSEM with Oxford/HKL Nordlys EBSD system. For EBSD unetched samples were used that had been polished to a 0.1 μm surface finishing using a colloidal silica suspension.

3. Results and Discussion

Figure 1a shows a sample from the 150-106 μm sieve fraction displaying a typical, fully dendritic morphology. The cooling rate for this sample, estimated using the methodology described in [23], is 7800 - 13000 K s^{-1}. In [24] the principal growth direction, for both the recalescence and post-recalescence material, was determined as <100> for solidification close to equilibrium. This is as expected for a material with the cubic L1$_2$ crystal structure. Normal <100> growth was observed to persist for cooling rates up to 26,000 K s^{-1}, (75 μm diameter droplets) wherein a transition to a mixed <100> and <110> growth mode was observed. It is clear that within the microstructure a large number of differently directed dendrites are present, which is highly suggestive of multiple nucleation events having occurred. The average grain size in these samples has been measured at 10.2 μm [24] and, with no evidence of dendritic fragmentation, it seems reasonable to assume that each grain originates from an independent nucleation event, giving an estimate nucleation density of 9.45×10^{14} m^{-3}. Even at the very highest cooling rates, $\geq 62,000$ K s^{-1}, for droplets ≤ 38 μm diameter, we still observe large numbers of grains per droplet. This is highly unusual as most other materials display only 1 grain per droplet at these very high cooling rates. Moreover, there is little evidence of porosity, either at the grain boundaries or in the interdendritic space, suggesting minimal solidification shrinkage.

Figure 1b shows an EDX line scan across one of the dendrite trunks. It is clear that, to within the normal errors associated with EDX, there is no difference in composition between the dendrite and the surrounding interdendritic material, as would be expected for a congruently melting compound. In addition, XRD analysis confirms that all of sieve fractions comprise single phase β-Ni$_3$Ge, with all of the diffraction peaks being unambiguously matched to ICCD reference pattern 04-004-3112 for β-Ni$_3$Ge. Etching normally produces topographic contrast resulting from differential dissolution due to differences in either phase or composition. Accordingly, the question here is what produces that topographic contrast in a single phase sample of homogeneous composition. In fact, we show in [25] that the contrast arises due to the degree of local chemical ordering present, with the dendrites being disordered and the surrounding material being ordered. Such a situation would arise due to disorder trapping in the rapidly solidified material growing during recalescence, with the interdendritic material growing more slowly, and hence as the ordered phase, post-recalescence. This would be consistent with the known resistance of intermetallic compounds to chemical attack, with the disordered, and hence more metallic, phase preferentially dissolving in the aggressive etch used here. The upshot is the rare

situation in which etching will reveal only the solid formed during recalescence, leaving the post-recalescence solid unetched. Consequently this is, as far as we are aware, a unique material insomuch as it permits direct imaging of the solid formed during recalescence in the as-solidified sample.

As described above, droplets in the 150-106 μm sieve fraction display an as-solidified microstructure which is typically of dendritic solidification in a cubic material. For the smaller sieve fractions, and hence higher cooling rates, a number of microstructural changes are observed including a change in the dendrite growth direction and the occurrence of seaweed structures. However, it is the large sieve fractions, and hence lower cooling rates, that are of interest here.
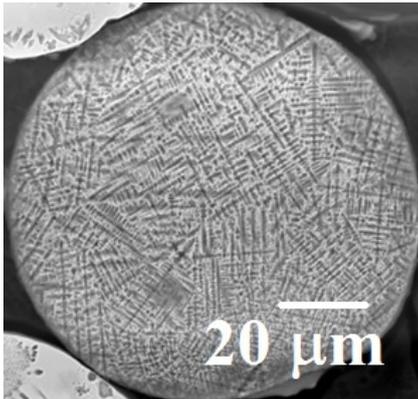
Figure 1. Typical microstructure as observed in a sample of drop-tube processed β-Ni$_3$Ge from the 150-106 μm sieve fraction following etching in a mixture of HF + HCl + HNO$_3$. Numerous, multiply branched dendrites are observable. Contrast arises due to preferential etching of the ordered material formed during the recalescence phase of solidification.

Figure 2a shows a typical sample from the 300-212 μm sieve fraction (cooling rate 2800 – 4600 K s^{-1}). Numerous linear arrays of near spherical fragments are evident. We believe that such linear arrays of particles could only arise by the melting, and subsequent spheroidisation of primary dendrites. Typical fragment size in these arrays is 5-10 μm Moreover, in Figure 2b, now taken from the 212-150 μm sieve fraction, the higher cooling rate, estimated as 4600 - 7800 K s^{-1}, appears to have resulted in a dendrite being captured in the process of fragmenting. Specifically, the uppermost secondary arm on the left-hand side of the micrograph has detached from the primary trunk and appears to have undergone almost complete fragmentation into 6 more-or-less distinct spherical fragments while the secondary arm below this displays the modulation characteristic of the onset of the Rayleigh instability. The mean fragment diameter in the fully fragmented arm in the top left of the image is ≈ 2.4 μm. As the nature of the contrast in these samples is between the rapidly solidified (chemically disordered) material and that solidified close to equilibrium (chemically ordered) material, there is unfortunately no means to distinguish between material that grew post-recalescence and material that grew during the recalescence phase of solidification but subsequently remelted. Both ultimately solidified close to equilibrium and hence will be the chemically ordered phase.
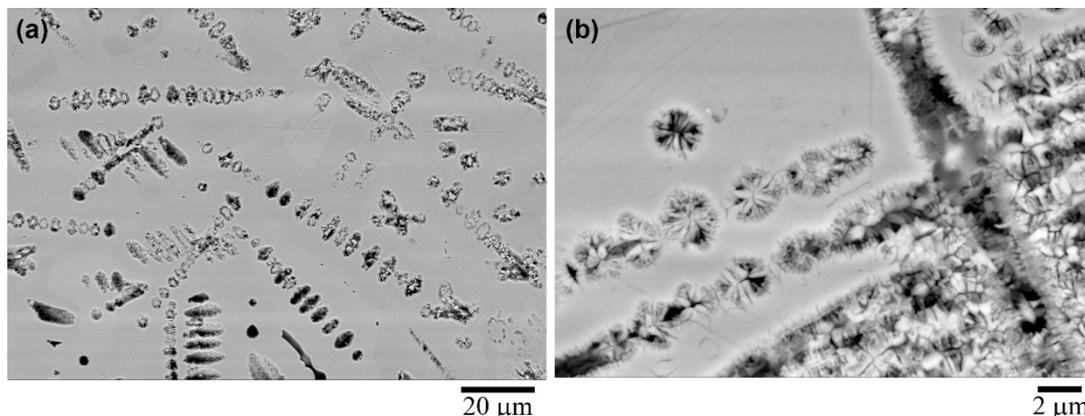
Figure 2. SEM micrograph of fragmented dendrites β-Ni$_3$Ge from (a) the 300-212 μm sieve fraction and (b) the 212-150 μm sieve fraction.

Based on the evidence present above we contend that in rapidly cooled β-Ni₃Ge there exist a range of cooling rates, and therefore plateau times, τ_{pl}, in which the fragmentation of dendrites may be observed directly in the as-solidified microstructure. Such fragmented dendrites appears to be the dominant morphology in the 300-212 μm sieve fraction, for which τ_{pl} is estimated to be in the range 0.22-0.12 s (corresponding to the upper and lower sieve limits respectively). In the next sieve size down, 212-150 μm, wherein τ_{pl} = 0.12-0.06 s respectively, partial fragmentation, particularly now of the secondary dendrite arm may still be observed, while for all smaller sieve fractions such fragmentation appears to be wholly inhibited by the high cooling rate. Given that we can now, with reasonable certainty, conclude that dendritic fragmentation is occurring, the pertinent question becomes are these samples also grain refined. The polished and etched samples do not display obvious grain boundaries, so we have used EBSD to investigate the grain size distribution.

Figure 3a shows an EBSD Euler orientation map from a sample in the 300-212 μm sieve fraction, i.e. in which fully fragmented dendrites are expected to be the dominant morphology. The EBSD map reveals there are a small number of large grains, typically > 50 μm, with a much larger number of small grains in the size range 5-10 μm. Interestingly, the large grains all appear to dappled with small regions of material displaying different crystallographic orientations to the main grain within which they are embedded. From this it would appear that some of the dendritic fragments give rise to small grains of < 10 μm diameter, but that many do not, instead being incorporated into much larger grains despite an obvious mismatch in orientation. The observed structure, comprising mixed large and small grains is does not resemble the classic SGR microstructure of uniformly distributed fine grains. For completeness we also show, in Figure 3b, an EBSD map characteristic of the 212-150 μm sieve fraction. Given that, from the SEM micrographs, dendrite fragmentation is unlikely to be complete, with primary trunks and some secondary arms intact, we may not expect to observe a grain refined structure. As with the larger sieve fraction the structure remains a mixture of large and small grains, although without the dappling of the large grains evident in the 300-212 μm sieve fraction.
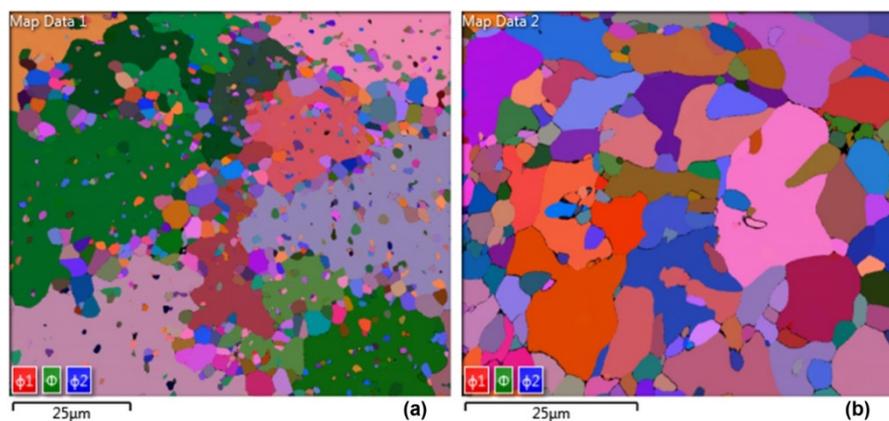
Figure 3. EBSD Euler maps obtained from β-Ni₃Ge in (a) the 300-212 μm sieve fraction and (b) the 212-150 μm sieve fraction. Note in (a) the large number of small fragments that appear to have been incorporated into much larger grains.

We have then a system in which we can establish that dendritic fragmentation occurs over a certain well defined range of cooling rates. However, such fragmentation does not appear to be a particularly effective mechanism for grain refinement. It appears that some fragments are likely to nucleate fine grains, as evidenced by the large number of small grain in the EBSD map for the 300-212 μm sieve fraction, but this does not seem to be pervasive, with many large grains remaining. Indeed, > 90% of the field of view in the EBSD map (≈8750 μm²) is occupied by just 12 grains. Consequently, the resulting structure is not the one typically associated with SGR. We note that for droplets in free-fall in the drop-tube flow in the melt is likely to be suppressed and we believe it is possible that if flow were present to

disperse the fragments, grain refinement by dendritic melting may be more effective. In this regard we note that electromagnetic levitation induces strong flow within the melt and that this has been shown to influence the results obtained by this technique [26]. However, in such a case it is questionable whether SGR by dendrite fragmentation should be considered an inherent property of the material or a consequence of the processing technique. This would also not account for the many samples observed to display SGR processed by techniques which do not induce extensive flow in the melt (melt fluxing, drop-tube, electrostatic levitation). We conclude the dendrite remelting and fragmentation is not an efficient cause of SGR.

4. Summary and Conclusions

The rapid solidification of single-phase, congruently melting β-Ni_3Ge has been studied in by drop-tube processing. Rapid growth during the recalescence phase of solidification results in a disordered solid which may be etched preferentially to the ordered solid that grows post-recalescence. Over a range of cooling rates from 2800 - 7800 K s^{-1} dendrites fragmented due to remelting may be observed directly in the as-solidified samples. However, despite containing many fully fragmented dendrites these samples do not display the grain size distribution normally associated with spontaneous grain refinement. We therefore conclude that the remelting and fragmentation of dendrites is not an efficient route to spontaneous grain refinement in deeply undercooled melts.

References
[1]   Walker J L 1959 *The Physical Chemistry of Process Metallurgy Part 2* ed G L St. Pierre (New York: Interscience) 845
[2]   Wilnecker R, Herlach D M and Feuerbacher B 1989 *Phys. Rev. Lett.* **62** 2707
[3]   Battersby S E, Cochrane R F and Mullis A M 1997 *Mater. Sci. Eng. A* **226** 443
[4]   Dragnevski K I, Cochrane R F and Mullis A M 2004 *Mater. Sci. Eng. A* **375-377** 479
[5]   Battersby S E, Cochrane R F and Mullis A M 2000 *J. Mater. Sci.* **35** 1365
[6]   Lu S Y, Li J F and Zhou Y H 2007 *J. Crystal Growth* **309** 103
[7]   Zhang T, Liu F, Wang H F and Yang G C 2010 *Scripta Mater.* **63** 43
[8]   Matson D 1998 *Solidification 1998* eds S P Marsh, J A Dantzig, R Trivedi, W. Hofmeister, M G Chu, E J Lavernia and J-H Chun (Warrendale PA: TMS) 233
[9]   Castle E G, Mullis A M and Cochrane R F 2014 *Acta Mater.* **66** 378
[10] Castle E G, Mullis A M and Cochrane R F 2014 *Acta Mater.* **77** 76
[11] Kattamis T Z and Flemings M C 1967 *Mod. Casting* **52** 97
[12] Powell G L F and Hogan L M 1969 *Trans. AIME* **245** 407
[13] Southin R T and Weston G M 1973 *J. Aust. Inst. Met.* **18**
[14] Horvay G 1962 *Proc. of the 4 US National Congress of Appl. Mech.* (Univ. California) 1315
[15] Schwarz M, Karma A, Eckler K and Herlach D M 1994 *Phys. Rev. Lett.* **73** 1380
[16] Karma A 1998 *Int. J. Non-equilibrium Process.* **11** 201
[17] Mullis A M, Dragnevski K and Cochrane R F 2004 *Mater. Sci. Eng. A* **375-377** 157
[18] Heringer R, Gandin Ch-A, Lesoult G, Henien H 2006 *Acta Mater.* **54** 4427.
[19] Chen J, Dahlborg U, Bao C M, Calvo-Dahlborg M and Henien H 2011 *Metall. Mater. Trans. B* **42** 557.
[20] Nash A and Nash P 1976 *US National Bureau of Standards Monograph Series 25*, (Ohio:Elsevier, ASM) 35
[21] Ahmad R, Cochrane R F and Mullis A M 2012 *J. Mater. Sci.* **47** 2411
[22] Cao L, Cochrane R F and Mullis A M 2015 *Metall. Mater. Trans. A* **46** 4705
[23] Oloyede O, Bigg T D, Cochrane R F and Mullis A M 2016 *Mater. Sci. Eng. A* **654** 143
[24] Haque N, Disorder Trapping in Rapidly Solidified Intermetallic Compounds, PhD Thesis submitted to the University of Leeds, July 2018.
[25] Haque N, Cochrane R F and Mullis A M 2016 *Intermetallics* **76** 70
[26] Binder S, Galenko P and Herlach D M 2014 *J. Appl. Phys.* **115** 053511